J Mater Sci (2018) 53:2618–2630

Electronic materials

Low-pressure solid-state bonding technology using fine-grained silver foils for high-temperature electronics

Jiaqi Wu[1,2,*] and Chin C. Lee[1,2]

[1] *Electrical Engineering and Computer Science, University of California, Irvine, CA 92697-2660, USA*
[2] *Materials and Manufacturing Technology, University of California, Irvine, CA 92697-2660, USA*

Received: 30 June 2017
Accepted: 6 October 2017
Published online: 12 October 2017

ABSTRACT

A solid-state bonding technique using fine-grained silver (Ag) foils is presented. The Ag foils are manufactured using many runs of cold rolling and subsequent annealing processes to achieve the favorable microstructure. X-ray diffraction and pole figure measurement are performed to examine the crystal structure and grain orientations. Si chips are bonded to bare Cu substrates using the Ag foil as the bonding medium at 300 °C in 0.1 torr vacuum assisted by 6.9 MPa static pressure, which is much lower than that used in conventional thermal compression bonding. Cross sections prepared by focus ion beam show clear bonding interfaces with only a few voids smaller than 100 nm. The bonded structures do not crack after cooling down to room temperature, indicating that the ductile Ag layer is able to manage the strain induced by the large coefficient of thermal expansion mismatch between Si and Cu. The average shear strength of as-bonded samples is 29 MPa. High-temperature storage tests are conducted, and slight increase in strength can be observed after 300 °C aging. Fracture analyses show that the breakage occurs within the Ag foil rather than on the bonding interface. Transmission electron microscopy and energy-dispersive spectroscopy (TEM/EDX) are conducted for Ag/Cu interface after 200-h aging, and the result shows that slight diffusion proceeds during the aging. Since Ag has the highest electrical and thermal conductivities among metals, therefore the bonded structures reported in this paper probably represent the best possible design for high-temperature and high-power electronic packaging applications.

Introduction

In electronic packaging, die-attach is a crucial step that provides active devices with mechanical support and heat dissipation path. Nowadays, advanced development in aircraft, automotive, aerospace, and deep oil and gas drilling requires electronic devices to operate at high temperature. For example, the operating temperature of devices in deep oil exploration has increased to 300 °C [1]. Traditional high-

Address correspondence to E-mail: jiaqw10@uci.edu

DOI 10.1007/s10853-017-1689-y

temperature die-attach materials such as gold-germanium (AuGe) eutectic alloy and high-lead (Pb) solder cannot sustain this temperature because their melting temperatures are not high enough. On the other hand, materials with high melting temperature require high process temperature to turn them into molten phase during bonding. One method to circumvent this constraint is the solid–liquid interdiffusion bonding (SLID) that employs a structure consisting of a low-melting-point component and a high-melting-point component [2]. During bonding, the low-melting-point component melts and is consumed by reacting with the high-melting component to form a new phase that has high melting temperature. Thus, high-temperature joints can be made at low bonding temperature. SLID processes based on Ag/Sn [3], Cu/Sn [4, 5], and Au/Sn [6] had been developed. A concern on SLID joints is the intermetallic compound (IMC) region formed when the molten phase is consumed during bonding. Although the mechanical properties of IMC joints can be improved through post-heat treatments [7, 8], the formation of pores is an issue. Ga and In had also been used in SLID designs due to its low melting temperature. SLID joints made with Ag/In [9, 10] and Cu/Ga [11, 12] systems had been reported, where the IMC formation issue persists. A technique to eliminate the IMC region is to convert it into a solid solution phase by post-annealing, as demonstrated using the Ag/In system [13]. The resulting joints between Si chips and Cu substrates survive 5000 thermal cycles between − 40 and + 200 °C.

A recent approach to producing high-temperature joints is to sinter nano-silver paste where Ag nanoparticles dispersed in binder agglomerate during sintering. A recent report shows that as the size of Ag nanoparticle scales down to 2.4 nm, the surface pre-melting temperature can be as low as 350 °C due to increased proportion of atoms on the surfaces [14]. With further process improvements, the sintering temperature has been reduced to 275 °C [15]. A fundamental challenge of sintered Ag process is the pores that cannot be eliminated. In high-temperature reliability tests, many research groups had reported the penetration of oxygen through the pores within the Ag to reach Cu substrates, producing an oxide layer which becomes the weak region [16, 17]. A few groups have developed coating methods on the substrates to reduce oxidation. However, the interdiffusion between metallized layers and porous silver can enlarge the pore size near the interfacial region, resulting in bonding strength degradation [15, 18].

Regardless of pores in sintered Ag, Ag is still an attractive bonding medium because of its superior physical properties: the highest electrical conductivity (63×10^6 S/m) and highest thermal conductivity (429 W/m–K) among metals, high melting temperature, and high ductility. Furthermore, based on Ag–Cu phase diagram shown in Fig. 1 [19] (the diagram was colored by ASM International 2012, http://mio.asminternational.org/apd/index.aspx), Ag and Cu do not form IMCs. This is in contrast to nearly all soldering and SLID processes where the IMC formation is essential [20]. Since Cu is the most commonly used material for leadframes, electrodes, and bond pads in electronic packaging, high-quality joints of semiconductor chips to Cu using Ag would be of significant contribution to electronics in general and to high-temperature power electronics in particular. In this research, we turn to solid-state atomic bonding idea for which atoms on the bonding interface must be brought within atomic distance in order for bonding to occur [21]. To facilitate this condition, the materials on the interface must deform and mate to each other to achieve atomic contact. To make Ag deform more easily, Ag foils are produced through cold rolling and subsequent annealing many times to obtain favorable microstructure. During bonding, pressure of 1000 psi (6.9 MPa) is applied at 300 °C to further enhance the deformation of Ag surface. It is worthwhile to indicate that this pressure is a few orders smaller than the pressure used in industrial thermo-compression bonding processes [22].

In the following sections, the preparation and characterization of silver foil will be firstly introduced. Secondly, the process of solid-state bonding will be briefly described. Next, the cross-section images will be shown and quality of joints evaluated. In addition, shear tests will be performed for strength evaluation before and after high-temperature storage (HTS) tests. Lastly, the potential application and scientific value will be discussed.

Experimental design and procedures

To produce Ag foils, Ag ingots are first grown by melting Ag shots under vacuum, followed by natural cooling down to room temperature. Several runs of cold rolling and subsequent annealing are then

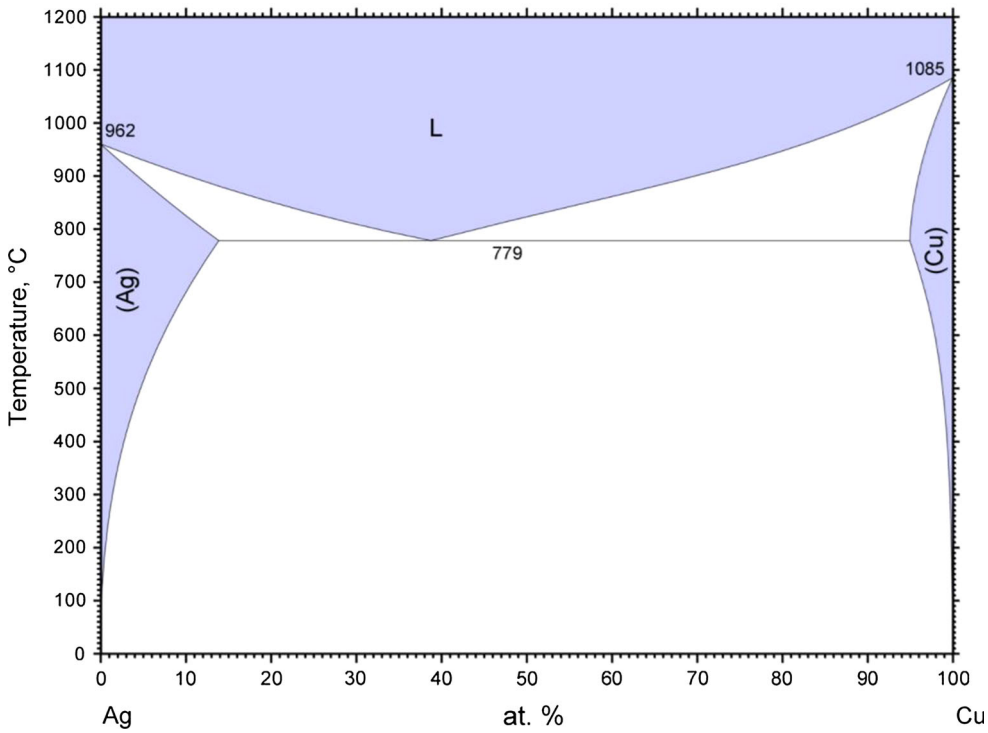

Figure 1 Ag–Cu binary phase diagram [19].

performed to reduce the thickness of an ingot. As it was mentioned in the previous section, Ag foil needs to be soft enough to be deformed easily during the bonding process. A recent report also demonstrated that the ease of dislocation gliding facilitates the collapse of surface asperities during solid-state bonding [23]. Therefore, grains with low dislocation density are preferred, which can be acquired after recrystallization [24]. On the other hand, the initial grain size of the ingot ranges from hundreds of microns to a few millimeters, refinement of grains is necessary since the thickness of the foil is within 100 μm. Therefore, these rolling and annealing conditions are determined after many rounds of trials and adjustments. In each run, the thickness is reduced by 70%, and the annealing temperature is optimized at 300 °C, corresponding to a homologous temperature of 0.46 at which recrystallization is expected to complete and excessive grain growth does not occur within 1 h [25]. The final foil thickness is approximately 75 μm, suitable for bonding experiments. Prior to each bonding experiment, the foil is slightly polished by 1 μm diamond suspension solution and rinsed with deionized water.

In general, metallic materials become harder and less ductile after cold work because the heavy increase in dislocation density makes dislocations harder to glide within crystal grains [26]. In addition, texture is formed within polycrystalline metals during cold rolling, making the materials exhibit certain anisotropy in mechanical properties. In this research, an isotropic and texture-free Ag foil microstructure is highly preferred since the Cu electrode and substrates used in electronics do not have a preferred orientation. To confirm that residue stress and texture are removed by the annealing process, X-ray diffraction (XRD) and pole figure (PF) measurement are conducted using Rigaku Smartlab in Irvine Materials Research Institute (IMRI) [27]. XRD theta–theta scan is operated using Bragg–Brentano (BB) optics at 2° per minute with a filter removing K-beta line. In-plane parallel beam (IPB) scan is performed for PF measurement. An as-rolled foil sample without final annealing is chosen as the control group only for PF experiment.

To produce the semiconductor chips for bonding experiments, 3-inch silicon (Si) wafers are deposited with 30 nm Cr and 100 nm Au thin films by E-beam evaporation in one high vacuum cycle (5×10^{-6} -torr). The Cr provides strong adhesion between Si and Au. The Au layer protects Cr from oxidation and works as a bonding buffer as it does not oxidize. The Si wafers are then diced into 5 mm × 5 mm chips and ready for bonding. Cu substrates of

7 mm × 7 mm are cut from a Cu sheet purchased from a vendor. Right before bonding, they are slightly polished by 1 μm diamond powder suspended solution and rinsed with thin hydrochloric acid and DI water to remove the oxides and contaminants.

The bonding structure design is illustrated in Fig. 2. The metallized Si chip, Ag foil, and Cu substrates are held together by a fixture with a pressure of 1000 psi (6.9 MPa) onto a graphite heater stage in a vacuum chamber [28]. The chamber is pumped to 0.1 torr, and the graphite stage is heated to 300 °C in 5 min, kept isothermally for 5 min, and cooled down naturally in vacuum to room temperature. The vacuum environment reduces Cu oxidation during the bonding process.

To evaluate the joint quality, the samples are mounted in epoxy resin, cut in cross sections, and polished. Optical microscope (OM) and Tescan Gaia3 SEM–FIB in Irvine Materials Research Institute (IMRI) are utilized for cross-section examination. Since mechanical polishing process often causes smearing of materials over the interface, focus ion beam (FIB) cutting is applied onto the interface to produce a true interface in atomic scale without smearing. Furthermore, the in-beam backscattered electron (BSE) signal enables us to obtain crystallographic orientation contrast imaging on the cross section, resulting in images showing microstructure with detailed crystalline grains. High-temperature storage (HTS) tests at 300 °C are performed, following the process specified in JESD22-A103E [29]. After that, the cross sections of all samples tested are examined by the same FIB cutting and SEM imaging process. To further study the structure evolution of Ag–Cu interface during aging, TEM sample is cut from sample after 200-h aging by FIB. Bright field (BF) imaging and EDX are conducted for interfacial morphology examination and composition analysis.

To evaluate the strength of the samples, shear test is conducted using Nordson Dage 4000 tester at a shear speed of 500 μm/s for as-bonded samples and for the samples after HTS aging. After the shear test, the fracture surfaces are examined by SEM to reveal the deformation morphology and the fracture modes.

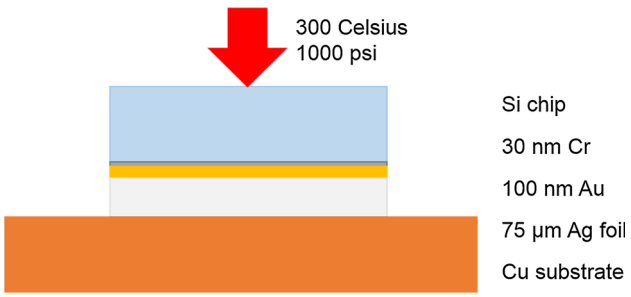

Figure 2 Illustration of bonding structure (dimensions of small features are exaggerated).

Experimental results and discussions

XRD and PF measurement

XRD result of a typical as-annealed Ag foil is shown in Fig. 3. The data collected in the test are processed and analyzed by PDXL, an integrated polycrystalline XRD analysis software package. The peaks in Fig. 3 are indexed, and the crystallographic information is sorted and listed in Table 1.

From Fig. 3, it is clear that the crystal structure of the Ag foil is face-centered cubic (FCC) in terms of the diffraction peaks' systematic absence. Several peaks associated with Cu were also detected because the Ag foil was attached to a Cu sheet during the scan process. In Table 1, d is the d-spacing of corresponding crystallographic planes, (hkl) is the Miller's indices with classical denotation, and a is the calculated lattice constant. The deduced lattice constant of 4.088 Å fits with the data recorded in ICDD card (03-

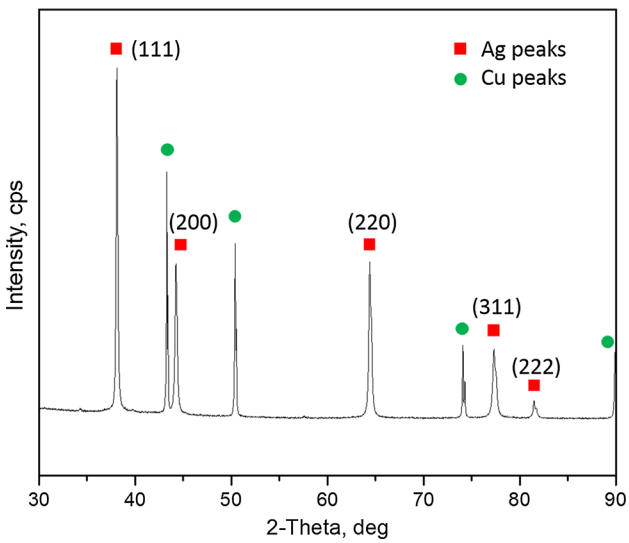

Figure 3 XRD pattern of a typical annealed Ag foil, where the Cu peaks were caused by X-ray incident on the Cu sheet on which the Ag foil was adhered to.

Table 1 XRD peaks and analysis results

Peak #	2-Theta (°)	*d* (Å)	(*hkl*)	*a* (Å)
1	38.10	2.359	(111)	4.088
2	44.23	2.045	(200)	4.090
3	64.39	1.445	(220)	4.087
4	77.32	1.233	(311)	4.088
5	81.48	1.180	(222)	4.087

065-2871) perfectly with only 0.5% deviation, an indication of Ag material nearly free from macroscale residue stresses.

The PF measurement results of as-rolled and as-annealed samples are exhibited in Fig. 4. Figure 4a, b shows that the (111) poles of an as-rolled sample are concentrated near 45° and the (220) poles are concentrated near 90°, which are consistent with the theoretically calculated results based on mechanics and the operation of slip systems in FCC polycrystalline metals with low stacking fault energy [30]. From Fig. 4c, d, it is seen that the concentration of (111) poles and (220) poles is greatly reduced after annealing, which indicates that the strain energy stored during cold work was released to trigger recrystallization resulting in a near texture-free microstructure.

The XRD and PF measurement results presented are representative and repeatable for silver foils from different batches. In conclusion, high-quality, stress-free, and near texture-free silver foils have been successfully prepared by cold rolling and subsequent annealing processes.

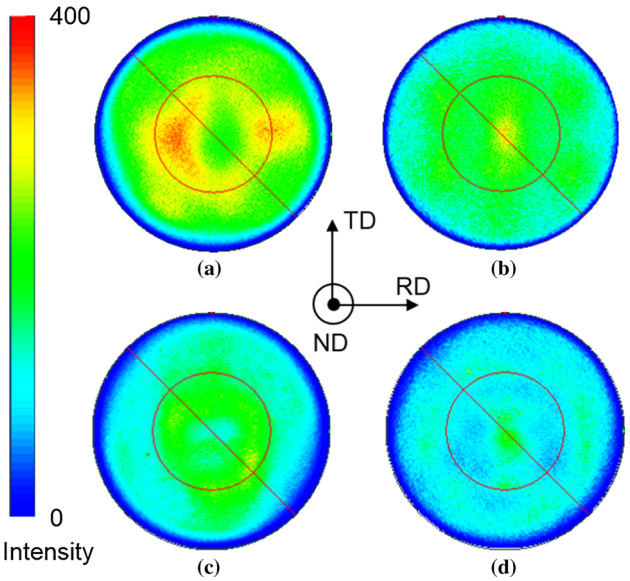

Figure 4 PF measurement results: **a** (111) poles of as-rolled sample, **b** (220) poles of as-rolled sample, **c** (111) poles of annealed sample, **d** (220) poles of annealed sample.

Cross-section examinations of as-bonded Si/Ag/Cu structures

According to Fig. 5, the Si/Ag and Ag/Cu bonding interfaces are clear and sharp without defects under optical microscope inspection. Given the large difference in coefficient of thermal expansion (CTE) between Cu (17×10^{-6}/ °C) and Si (2.7×10^{-6}/ °C), the crack-free silicon implies that the ductile Ag layer is capable of managing the strains induced by the CTE mismatch. It is worth reminding that the Si chips were coated with thin Cr and Au layers. It is the Au layer that bonds to the Ag foil. To study the Ag/Cu bonding interface, it is a challenge to produce a clear and sharp interface using mechanical polishing processes because of smearing effects of ductile Ag and Cu during polishing. We thus turned to FIB cutting to produce a clear and sharp interface. Figure 6a displays the high-magnification SEM image of the FIB-cut interface. The bonding interface is clear and sharp. No IMCs are observed near the interface, as suggested by the Ag–Cu phase diagram. There are a few voids less than 100 nm in size, probably caused by contaminations as the samples were prepared in a typical laboratory rather than in cleanroom environment. To quantify the fraction of voids along the interface, several images containing interface of 25 μm in total length have been captured and the number of the voids counted. The result is calculated to be 0.56/μm. Figure 6b is an SEM view showing the

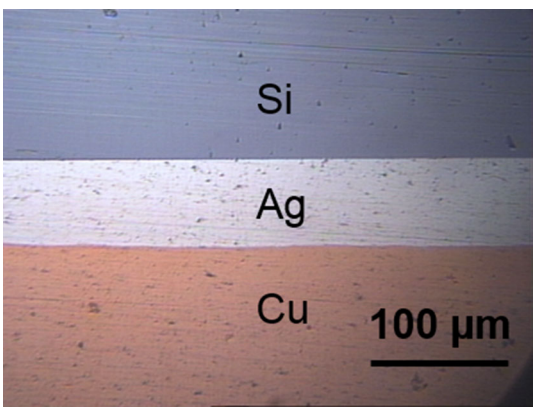

Figure 5 Optical microscopy image of an as-bonded Si/Ag/Cu structure.

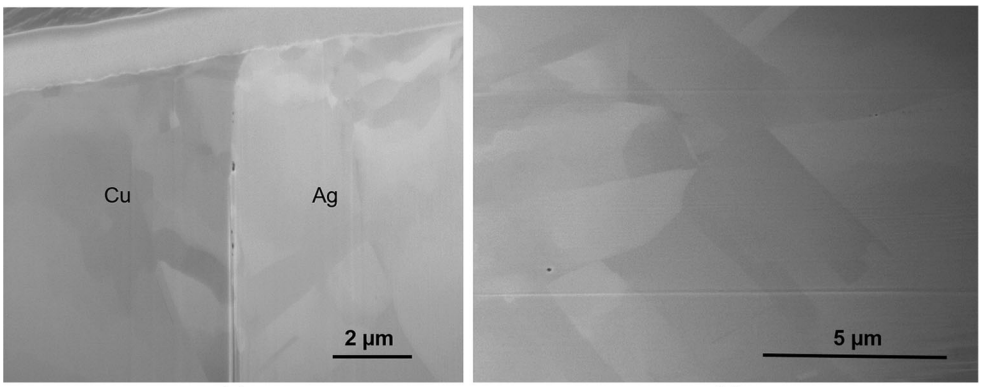

Figure 6 SEM images of interface region of a sample prepared by FIB cutting: **a** Cu/Ag bonding interface, **b** orientation contrast image on Ag region.

Ag grains in the foil. The grain size is within 5 μm, and the recrystallization was completed during the annealing process after cold rolling in consideration of the shape of these grains and the vanishing rolling textures as well.

HTS test results

The high-temperature reliability of joints was evaluated through HTS tests. Samples were aged at 300 °C for 72 and 200 h in air, respectively. Afterward, cross-section studies were performed following the same procedures as for as-bonded samples. OM and SEM images were captured and are shown in Figs. 7 and 8, respectively.

According to Fig. 7a, b, the joints remain at good conditions after long-term aging. The Si/Ag/Cu structure is still very clear, and no cracks are observed in Si chips. Figure 8 displays high-magnification SEM images after FIB cutting of aged samples. Figure 8a, c exhibits the Ag/Cu bonding interfaces, respectively, after 72- and 200-h aging. After such a high-temperature storage test, the bonding interfaces are still intact aside from a few voids of size less than 100 nm. The fraction of voids for these two conditions are measured to be 0.64 and 0.44/μm, respectively. No cuprous oxides or other compounds were found. This means that the bonding interface is so robust that no oxygen could penetrate through the Cu/Ag bond even at 300 °C. That is, the Cu/Ag interface is air-tight at 300 °C. This feature is important in applications where hermetic seal is required. Figure 8b is an orientation contrast SEM image on an Ag region after 72-h aging. The Ag grains are about 5 μm, similar to those on as-bonded sample. Figure 8d is an orientation contrast image after 200-h aging. It is observed that the Ag grains have grown to more than 10 μm with a preferred orientation. It is worth pointing out that the Ag foil thickness is 75 μm. Thus, further grain growth will be constrained by the foil thickness.

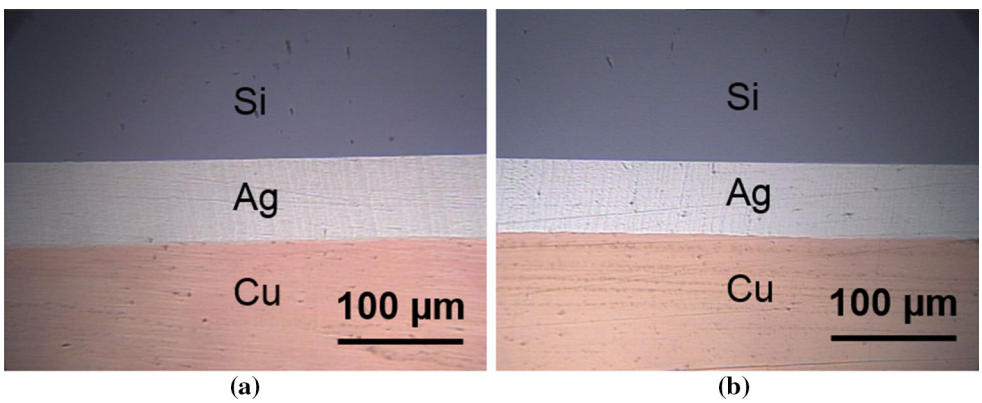

Figure 7 Cross-section OM images of samples after aging at 300 °C in air: **a** sample after 72 h, **b** sample after 200 h.

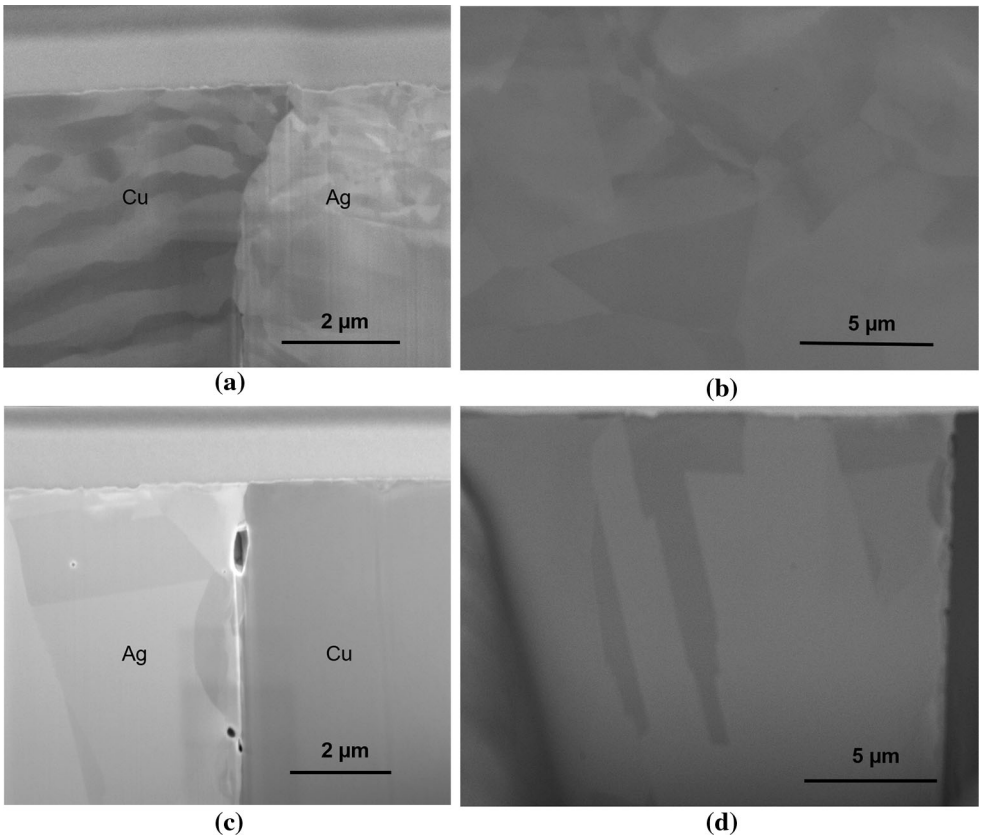

Figure 8 SEM images of cross sections produced by FIB cutting on samples after aging at 300 °C in air: **a** interfacial region after 72-h aging, **b** orientation contrast image of Ag region after 72-h aging, **c** interfacial region after 200-h aging, **d** orientation contrast image on Ag region after 200-h aging.

Shear test results, fractography and discussion

Regardless of how good the bonding interfaces look under optical microscope and SEM, the strength of samples is still unknown until it is measured. A commonly used method to determine the strength is the shear test, as illustrated in Fig. 9a. To perform shear tests, instead of using Si/Ag/Cu structures, we turned to Cu/Ag/Cu structures. The reason is that Si of the Si/Ag/Cu structure will break first during the test and the true strength of the structure cannot be determined. From our experience, a 5 mm × 5 mm Si chip cannot endure a shear force of 15 kgf applied to an edge by the shearing tool. Accordingly, a 5 mm × 5 mm Cu instead of a Si chip was bonded to a 7 mm × 7 mm Cu substrates using the same conditions to produce samples for the shear test. As-bonded samples, samples after 72-h aging and samples after 200-h aging were tested. There were 12

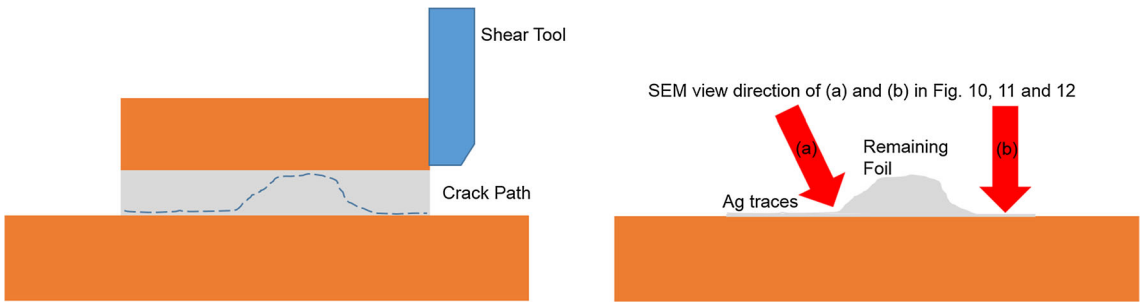

Figure 9 Configuration of shear test and illustration of fracture surface examination.

samples total, 4 per type. The average breaking load, corresponding shear strengths, and standard deviations are presented in Table 2. The results show that the strength of 3 types samples far exceeds the value (5 kgf) specified in American military standard (MIL-STD-883H method 2019.8) [31]. In addition, it is seen that the average breaking force actually increases a little after aging at 300 °C for 75 h and it increases further after aging for 200 h. That is, the strength is enhanced by the 300 °C aging process. This strengthening phenomenon further supports the idea that there is little oxygen penetration through the bonding interfaces to oxidize the Cu atoms on the interfaces. This is really a dream coming true: a structure that gets stronger during usage.

After preliminary inspection, the surface at which fracture incurred is similar for all samples, shown as the dash path on the cross-section sketch shown in Fig. 9a. To study the fracture in more details, all fractured samples were examined by SEM with view directions depicted in Fig. 9. The results of samples with three conditions indicated in Table 2 are presented in Figs. 10, 11, and 12, respectively.

From Fig. 10a, the broken end of the Ag foil is smooth with certain plastic deformation features. On the Cu substrate side, there are Cu regions and Ag-trace regions. The Cu regions have only Cu, indicating weak or no bonding between Ag and Cu. There are two types of Ag-trace regions. Figure 10b exhibits the region with Ag traces that have lots of submicron and micron size dimples. Figure 10c shows the region with Ag traces of cleavage nature. Figure 10d is an enlarged portion of Fig. 10c, exhibiting torn-apart appearance. For as-bonded samples, fracture occurred either within the Ag foil or near the Ag–Cu bonding interface but inside the Ag.

For a sample after 72-h aging, Fig. 11a shows that the broken end of the Ag foil appears similar to that of the as-bonded sample, but with a little bit more plastic deformation features. On the Cu substrate side, in addition to Cu regions, two types of Ag traces are found and circled as "c" and "d" in Fig. 11b. Region "c" region is enlarged as Fig. 11c, displaying dimples with size ranging from submicron to 5 μm. Region "d" is enlarged as Fig. 11d that exhibits cleavage features with very small dimples on top of them.

Figure 12a shows the broken end of the Ag foil of a sample after 200-h aging, where numerous deep dimples are observed on the ridge. On the Cu substrate side, the area of Cu regions has significantly reduced, as exhibited in Fig. 12b. This means that the area of no bonding or weak bonding on the Ag–Cu interface has decreased. Accordingly, the shear strength is expected to be higher, as indicated in Table 2. On the Ag traces, the dimples are more consistent and more uniformly distributed. Figure 12c, d is enlarged portions of Fig. 12b, where the dimple geometries indicate very ductile fracture.

The fracture evaluations presented above show that the joints become stronger and more ductile after aging. This can be attributed by interdiffusion and rearrangement of atoms within the interfacial region. Although interdiffusion is quite limited between Ag and Cu because of limited miscibility, it has been discovered that the grain boundary diffusion can proceed at elevated temperatures, as analyzed by ultraviolet photoelectron spectroscopy (UPS) depth profiling [32]. Figure 13a also shows the TEM image of Ag–Cu interface after 300-h aging. It is obvious that Ag and Cu mate each other very well without any oxides or compounds. EDX line scan is conducted along the red arrow, and the result is shown in Fig. 13b. It can be seen that small amount of Ag can be detected tens of nanometers away from the bonding interface, indicating that slight diffusion proceeds during the long-term aging. It is worth mentioning that Cu can also be detected on the Ag side; however, the intensity of signal cannot be directly related to concentration due to fluorescence since the TEM sample was welded on Cu grid. In conclusion, slight interdiffusion can proceed within

Table 2 Shear test results

Conditions	Average breaking load (kgf)	Average shear strength (MPa)	Standard deviation (MPa)
As-bonded	73.9	29.0	2.9
After 72-h aging	81.5	32.0	3.9
After 200-h aging	86.1	33.7	2.8

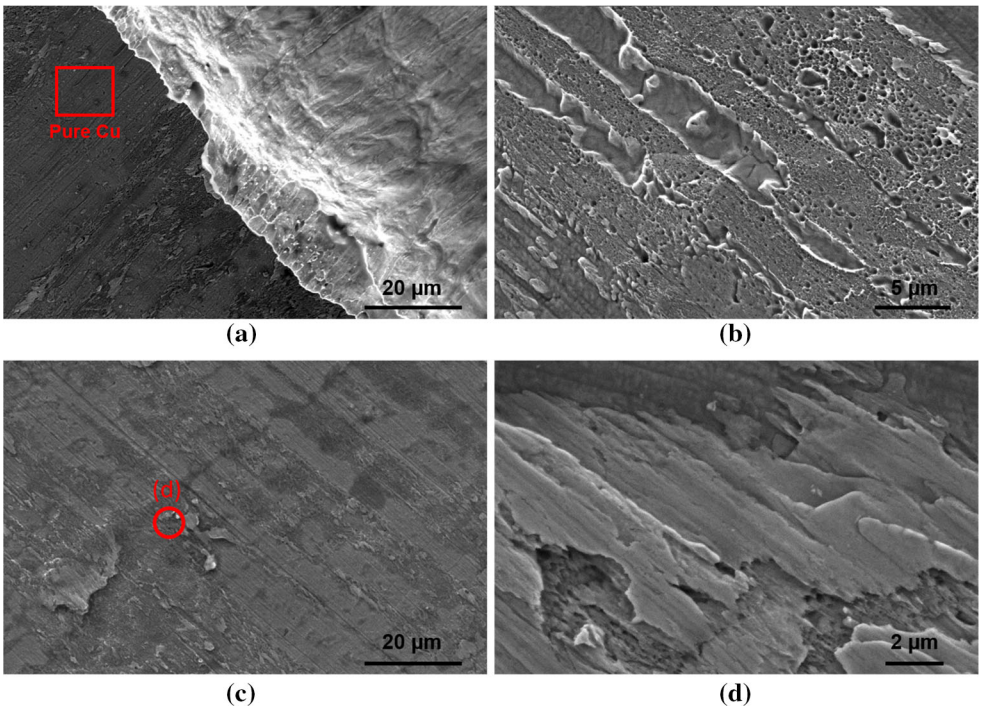

Figure 10 Fracture surfaces of an as-bonded sample: **a** overview of broken end of Ag foil and Ag traces on Cu substrate, **b** one type of morphology of Ag traces on Cu substrate, **c** another type of Ag traces, **d** high-magnification image of circled region in (**c**).

Figure 11 Fracture surfaces of a sample after 72-h aging at 300 °C: **a** overview of broken end of Ag foil, **b** overview of Ag traces on Cu substrate, **c** and **d** are high-magnification images of circled regions in (**b**).

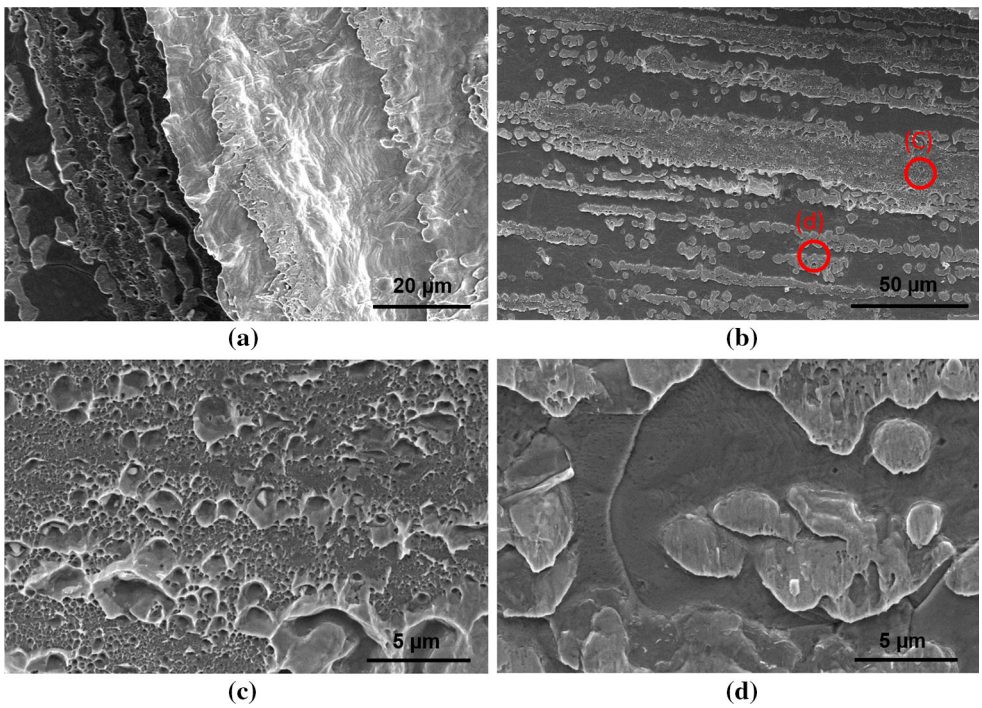

tens of nanometers near the interface during the aging process.

Furthermore, due to large difference in lattice constants and random orientation of grains on both sides of the interface, large quantity of crystal defects and residue stress are expected within the interfacial region such as vacancies and misfit dislocations at the initial stage. Given that the lattice misfit of Ag–Cu

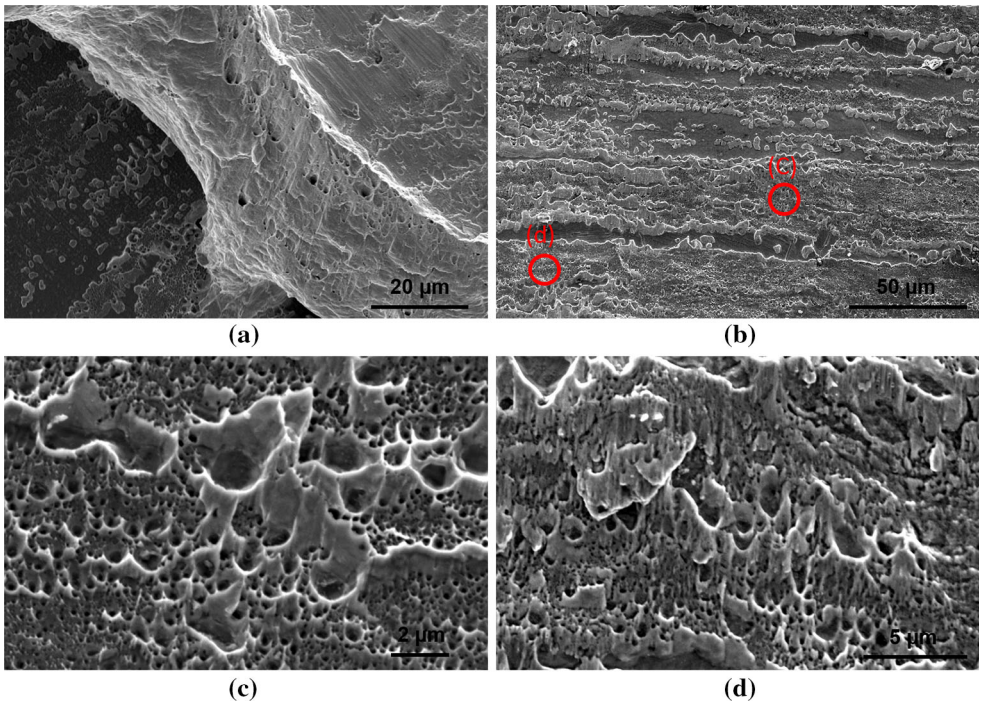

Figure 12 Fracture surfaces of a sample after 200-h aging: **a** overview of broken end of Ag foil, **b** overview of Ag traces on Cu substrate, **c** and **d** are high-magnification images of circled regions in (**b**).

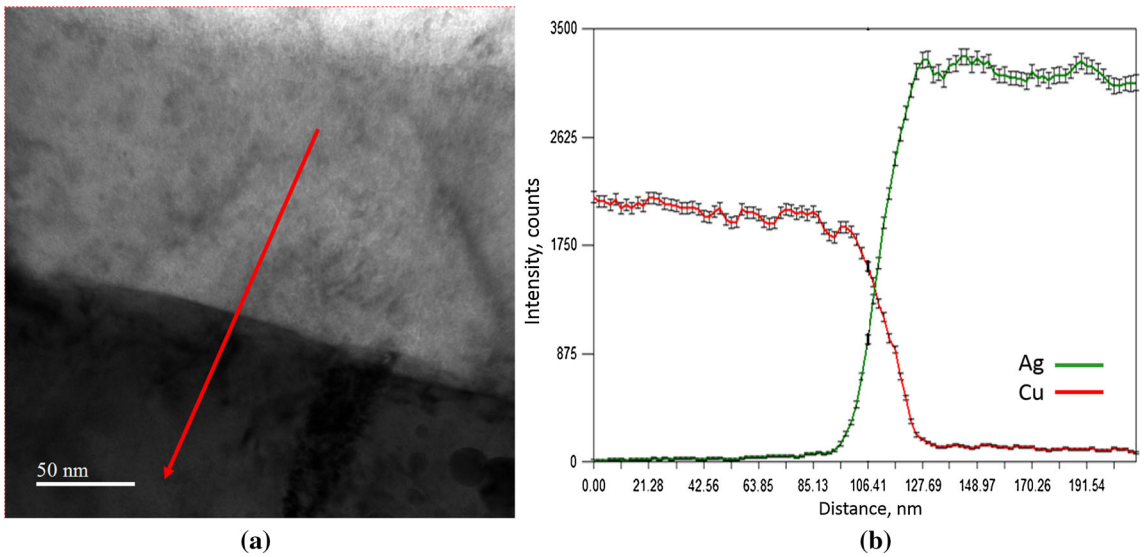

Figure 13 TEM analysis of Ag-Cu bonding interfaces after 200-h aging: **a** bright field imaging, **b** EDX line scan along the red arrow in (**a**).

system is 11%, coherent interface is not favorable in terms of strain energy penalty. Although there is no direct atomic resolution observation of Ag–Cu system so far, the Au–Cu interface may serve as a reference to understand the interfacial structure and the structure evolution during annealing because lattice misfit of the Au-Cu system is also 11%. The Au–Cu interface prepared by sputtering has been studied through high-angle annulus dark-field (HAADF) illumination which can provide atomic resolution Z-contrast imaging [33]. At the initial stage, both coherent phase boundary and incoherent region can be found. After annealing, the stress due to the lattice misfits is relaxed by the climb and glide of misfit dislocations. All these processes proceed within 20 nm near the interface. In total, although the initial state of our Ag–Cu interface is different from that of deposited Au–Cu, similar process may proceed to

facilitate the stress relaxation and to strengthen the interface after long-term aging. Another thing which is noticeable is that the fractured end of the Ag foil on the Cu substrate appears differently for samples after 200-h aging. This may be caused by different localized stress state during shear test given that the grain grows significantly after 200-h aging. In addition, excessive grain growth may result in loss of foil's strength. On the other hand, the strengthening in interfacial region during aging increases the overall strength of the samples. Fortunately, given that the thickness of foil is 75 μm, the space of grain growth is quite limited after 200-h aging. As a result, the Ag/Cu bonding interfaces are expected to be reliable for high-temperature applications.

It is interesting to compare our results with that of Ag–Cu joints produced by sintered silver technology. Figure 14 shows the comparison of our data and HTS results available in the literature so far [16, 17]. It can be seen that the sintered silver can produce strong joints at the initial state. However, the strength drops drastically after aging at 250 °C due to the growth of cuprous oxide. Since degassing paths are needed for the escape of resultant binders and organic compounds during the sintering process, numerous pores are formed in the sintered Ag joints. These pores are connected rather than isolated, allowing oxidizing species to penetrate through the network of pores to reach the Cu substrates. Although the oxidation issue might be mitigated by Au or ENIG coatings on the Cu substrates, the additional processes would increase the production cost. Also, the interdiffusion between Au and porous Ag may decrease the strength [15, 18]. In contrast, our Ag joints are pore-free. The Ag–Cu bonding interfaces are shown to be air-tight even at 300 °C. Accordingly, our Ag–Cu joints formed by solid-state bonding technology exhibit superior reliability after aging at 300 °C for 200 h.

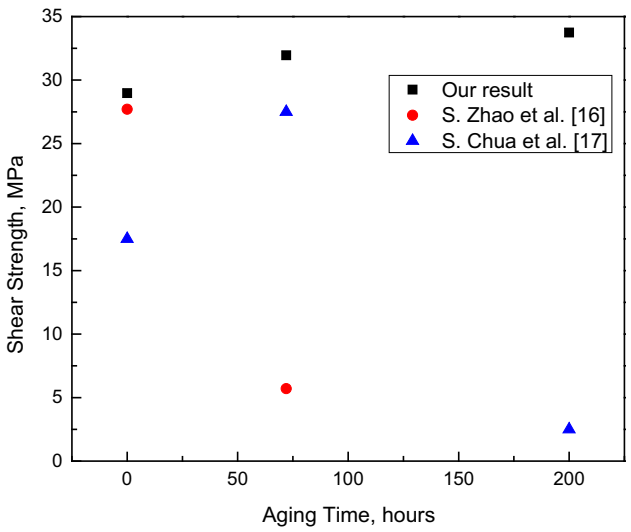

Figure 14 Strength comparison after HTS tests between our result and reports of sintered Ag technology (S. Zhao et al. conducted the aging at 250 °C) [16, 17].

Conclusion

Solid-state bonding technology using ductile Ag foil as the bonding medium has been developed. The fine-grained Ag foils were produced in house. Two structures, Si/Ag/Cu and Cu/Ag/Cu, were bonded at 300 °C with 1000 psi static pressure in 0.1 torr vacuum. The Si chips were coated with thin Cr and Au layers prior to bonding. HTS tests at 300 °C were conducted to evaluate long-term reliability. The Cu/Ag/Cu samples were used for shear test because the Si of the Si/Ag/Cu samples could not sustain much shear force. After shear test, fracture analyses were performed to evaluate the fracture surfaces and fracture modes. Major important results are summarized below:

1. Despite large CTE mismatch between Si and Cu, the Si/Ag/Cu structures did not break after cooling down to room temperature, indicating that the ductile Ag joint could manage the induced shear strains.
2. The breaking force of the joints is 74 kgf, far exceeding the 5 kgf requirement specified in Military Standard, MIL-STD-883H method 2019.8.
3. The corresponding average shear strength is 29 MPa. The shear strength increases for samples going through 300 °C storage tests, meaning that the structures are expected to get stronger during high-temperature usage.
4. The HTS test results indicate that the Ag/Cu bonding interfaces and Ag joints are air-tight, meaning that oxygen cannot penetrate through them even at 300 °C.
5. Fracture analyses reveal that the Cu/Ag/Cu structures broke within the Ag foil rather than on the Cu/Ag bonding interfaces.

It is well known that silver Ag has the highest electrical and thermal conductivities among all metals. Its melting temperature is as high as 962 °C. Accordingly, the solid-state bonding design reported in this paper probably not only represents the best possible design for high-temperature semiconductor device packaging applications but also can be applied in devices in which air-tight is required.

Acknowledgement

XRD, in-plane pole figure measurement, and SEM/FIB and TEM/EDX work were performed at UC Irvine Materials research Institute (IMRI).

References

[1] Beckwith R (2013) Downhole electronic components: achieving performance reliability. J Pet Technol 65:42–57

[2] Bernstein L (1966) Semiconductor joining by the solid-liquid-interdiffusion (SLID) process I. The systems Ag–In, Au–In, and Cu–In. J Electrochem Soc 113:1282–1288

[3] Li X, Cai J, Sohn Y, Wang Q, Kim W, Wang S, Microstructure of Ag–Sn bonding for MEMS packaging. In: 2007 8th international conference on electronic packaging technology, 2007, pp 1–5

[4] Li JF, Agyakwa PA, Johnson CM (2011) Interfacial reaction in Cu/Sn/Cu system during the transient liquid phase soldering process. Acta Mater 59:1198–1211

[5] Bosco NS, Zok FW (2004) Critical interlayer thickness for transient liquid phase bonding in the Cu–Sn system. Acta Mater 52:2965–2972

[6] Zhu ZX, Li CC, Liao LL, Liu CK, Kao CR (2016) Au–Sn bonding material for the assembly of power integrated circuit module. J Alloys Compd 671:340–345

[7] Li JF, Agyakwa PA, Johnson CM (2014) Suitable thicknesses of base metal and interlayer, and evolution of phases for Ag/Sn/Ag transient liquid-phase joints used for power die attachment. J Electron Mater 43:983–995

[8] Bosco NS, Zok FW (2005) Strength of joints produced by transient liquid phase bonding in the Cu–Sn system. Acta Mater 53:2019–2027

[9] Chuang RW, Lee CC (2002) Silver-indium joints produced at low temperature for high temperature devices. IEEE Trans Compon Packag Technol 25:453–458

[10] Wu YY, Lee CC (2013) High temperature Ag–In joints between Si chips and aluminum. In: 2013 IEEE 63rd electronic components and technology conference, 2013. pp 1617–1620

[11] Froemel J, Baum M, Wiemer M, Gessner T (2015) Low-temperature wafer bonding using solid-liquid inter-diffusion mechanism. J Microelectromech Syst 24:1973–1980

[12] Lin SK, Wang MJ, Yeh CY, Chang HM, Liu YC (2017) High-strength and thermal stable Cu-to-Cu joint fabricated with transient molten Ga and Ni under-bump-metallurgy. J Alloys Compd. 702:561–567

[13] Wu YY, Nwoke D, Barlow FD, Lee CC (2014) Thermal cycling reliability study of Ag–In joints between Si chips and Cu substrates made by fluxless processes. IEEE Trans Compon Packaging Manuf Technol 4:1420–1426

[14] Maruyama M, Matsubayashi R, Iwakuro H, Isoda S, Komatsu T (2008) Silver nanosintering: a lead-free alternative to soldering. Appl Phys A 93:467–470

[15] Xu QY, Mei YH, Li X, Lu GQ (2016) Correlation between interfacial microstructure and bonding strength of sintered nanosilver on ENIG and electroplated Ni/Au direct-bond-copper (DBC) substrates. J Alloys Compd 675:317–324

[16] Zhao SY, Li X, Mei YH, Lu GQ (2015) Study on high temperature bonding reliability of sintered nano-silver joint on bare copper plate. Microelectron Reliab 55:2524–2531

[17] Chua S, Siow KS (2016) Microstructural studies and bonding strength of pressureless sintered nano-silver joints on silver, direct bond copper (DBC) and copper substrates aged at 300 °C. J Alloys Compd 687:486–498

[18] Paknejad SA, Dumas G, West G, Lewis G, Mannan SH (2014) Microstructure evolution during 300 °C storage of sintered Ag nanoparticles on Ag and Au substrates. J Alloys Compd 617:994–1001

[19] Subramanian P, Perepezko J (1993) The Ag–Cu (silver–copper) system. J Phase Equilib 14:62–75

[20] Tu P, Chan YC, Lai J (1997) Effect of intermetallic compounds on the thermal fatigue of surface mount solder joints. IEEE Trans Compon Packag Manuf Technol B 20:87–93

[21] Lee CC and Cheng L (2014) The quantum theory of solid-state atomic bonding. In 2014 IEEE 64th electronic components and technology conference (ECTC). IEEE, pp 1335–1341

[22] Tofteberg HR, Schjølberg-Henriksen K, Fasting EJ, Moen AS, Taklo MM, Poppe EU et al (2014) Wafer-level Au–Au bonding in the 350–450° C temperature range. J Micromech Microeng 24:084002

[23] Chen G, Feng Z, Chen J, Liu L, Li H, Liu Q et al (2017) Analytical approach for describing the collapse of surface asperities under compressive stress during rapid solid state bonding. Scripta Mater 128:41–44

[24] Humphreys F (1997) A unified theory of recovery, recrystallization and grain growth, based on the stability and growth of cellular microstructures—I. The basic model. Acta Mater 45:4231–4240

[25] Callister WD, Rethwisch DG (2012) Fundamentals of materials science and engineering: an integrated approach. Wiley, Hoboken, pp 279–283
[26] Dieter GE, Bacon DJ (1986) Mechanical metallurgy. McGraw-Hill, New York, pp 231–233
[27] Irvine Materials Research Institute. http://www.imri.uci.edu/. Accessed 2017
[28] Lee CC, Wang DT, Choi WS (2006) Design and construction of a compact vacuum furnace for scientific research. Rev Sci Instrum 77:125104
[29] JESD22-A103E, High temperature storage life, JEDEC, 2015
[30] Dillamore IL, Roberts WT (1964) Rolling textures in f.c.c. and b.c.c. metals. Acta Metall 12:281–293
[31] MIL-STD-883H Method 2019.8, Die shear strength, Department of Defense, 2010
[32] Bukaluk A (1990) AES depth profile studies of interdiffusion in the Ag-Cu bilayer and multilayer thin films. Phys Status Solidi A 118:99–107
[33] Hartung F, Schmitz G (2001) Interdiffusion and reaction of metals: the influence and relaxation of mismatch-induced stress. Phys Rev B 64:245418